LIP-STUDENTS-23-18

Deciphering Jet Quenching Effects Using Novel Analysis Tools

Jay Nesbitt[1,a]

[1] *The University of Manchester, United Kingdom*

Project supervisors: Pablo Guerrero, Liliana Apolinário

October 20, 2023

Abstract. This work evaluates the validity of using the quantum mechanical formation time to select jets heavily modified by the quark-gluon plasma, with the aid of the newly proposed τ clustering algorithm. Unclustering jets with respect to formation time allows for an analysis of the jet's internal structure. The jet formation time is then compared to the opening angle and the groomed jet mass to study energy loss in the context of heavy-ion collisions. Our study is based on Z+jet events simulated by the JEWEL Monte Carlo event generator which includes jet quenching effects. This study concludes that the formation time has a greater discriminating power when it comes to jet selection in energy loss studies compared to the opening angle and groomed jet mass, which both induce a significant selection bias into the initial jet momentum. The formation time produces a significantly smaller bias, which alludes towards the prospective use of formation time pertaining to QGP probing in future studies.

Keywords: QGP, jet substructure, jet formation time, jet mass grooming, jet quenching.

1 Introduction

Quantum chromodynamics (QCD) describes the strong coupling sector of the Standard Model. For low virtuality/energy scale Q^2, colour confinement is observed, and for high Q^2, asymptotic freedom is observed: quarks and gluons, collectively named partons, can freely exist in hadrons under these short distance constraints. In proton-proton collisions, a parton contained within each proton may interact with each other, through the exchange of high energy gluons: this is a hard QCD scattering process. The partons involved in such a process will emit subsequent partons until Λ_{QCD}, a scale that limits applicability of perturbative methods [1]. At this scale partons will eventually hadronise[1], forming a collimated spray of hadrons, which is known as a jet. Jets are defined in terms of a jet algorithm and a recombination scheme. The former defines how the jet is clustered by iterating through the emissions from the parton shower, while the latter determines the momentum addition rules for determining the kinematics of the system of partons [2].

In the vacuum, the formation of jets can be very accurately described with perturbative QCD. As illustrated in the left side of Fig.1, such conditions can be assumed in proton-proton collisions, followed by a hadron gas phase and an eventual freeze-out. This evolution, however, is drastically different in heavy-ion collisions (HIC's), represented in the right side of Fig.1. After a HIC, the resulting system goes through an extremely short pre-equilibrium phase, followed by the formation of a Quark Gluon Plasma (QGP): a fluid-like state made of deconfined quarks and gluons [3, 4].

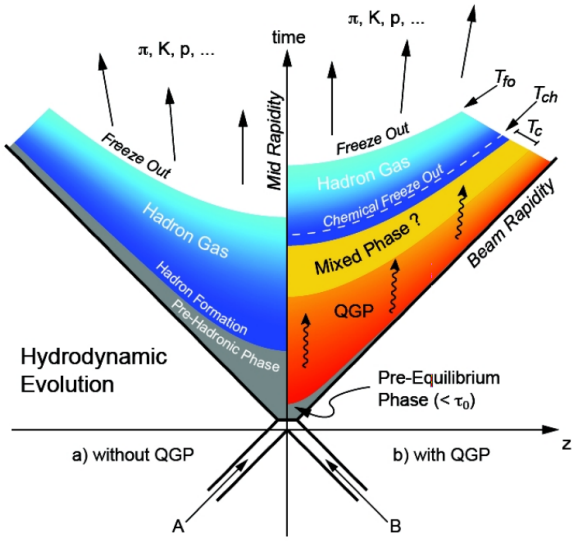

Figure 1. Minkowski Diagram of a) proton-proton collisions and b) HIC's [5].

The QGP existed in nature approximately 10^{-6} seconds after the Big Bang, and can be generated in laboratories such as the Relativistic Heavy Ion Collider (RHIC) and the Large Hadron Collider (LHC). RHIC collides gold nuclei at ultra-relativistic energies, producing significantly more final state particles than proton-proton collisions. The same can be said for the Large Hadron Collider (LHC), which collides samples of lead (Pb) nuclei at even higher energy scales than RHIC. This study exclusively details PbPb collisions. In these systems, the QGP exists for a very short time; once this state of matter is produced, it is followed by a rapid expansion. Then, once it reaches a critical temperature, the QGP particles will hadronise into final-state particles.

One ongoing field of research is using jet substructure to examine different QGP characteristics [6][7], which will in turn allow future studies to better describe the hydrody-

[a] e-mail: jaynesbitt21@gmail.com

[1] Hadronisation is a nonperturbative process, whose details are beyond the scope of this present study.

namics involved in the QGP phase of HIC's. Since QGP consists entirely of particles with colour charge, a jet (an object with colour charge) will interact with this state of matter, which leads to a suppression of the jet's cross section and a modification of the jet's internal structure. This phenomenon is collectively known as jet quenching.

The rapid expansion of QGP leads to a complex evolution of its state variables, such as temperature and pressure. As such, the amount of quenching a jet experiences will be convoluted with the time that the jet spends in the medium. When selecting jets that have been in the medium for a longer time (hence have more sensitivity to in-medium modifications), we propose an analysis of the jet's internal substructure. To access this information, we have to know how jets are constructed.

1.1 Jet Clustering

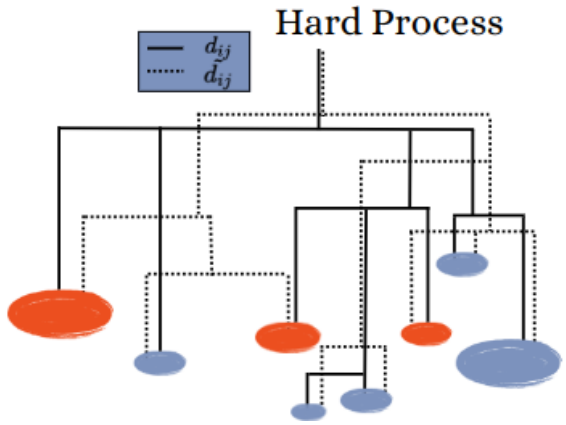

Figure 2. A visualisation of the clustering trees formulated by differing jet algorithms.

Jets are reconstructed from the 4-momenta of final state particles. There have been several different approaches to jet clustering proposed over the years. These approaches fall into two main categories: cone algorithms and sequential recombination algorithms [2]. We will focus on the latter for the purpose of this study; specifically, we will use the algorithm family known as the k_T family. This clustering algorithm family works via the following steps, for a single event. Firstly, the distances between all particles d_{ij}, which is given by are calculated, as well as d_{iB}. The distance between particles i and j is given by

$$d_{ij} = \min\left(p_{T1}^{2p}, p_{T2}^{2p}\right)\left(\frac{\Delta R}{R}\right)^2, \tag{1}$$

where p is the aforementioned parameter that dictates the form of the algorithm, R is the chosen jet radius, and

$$\Delta R = \sqrt{(y_1 - y_2)^2 + (\phi_1 - \phi_2)^2}, \tag{2}$$

where y is the rapidity and ϕ is the azimuthal angle. Meanwhile, the particle-beam distance is given by

$$d_{iB} = p_{Ti}^{2p}. \tag{3}$$

The minimum value from these distances is then selected. For a minimum d_{ij}, particle i and j are merged into a new particle k, with the above steps being repeated. If, however, the beam distance d_{iB} is the shortest distance, then object i is classified as a jet, and removed from the sample. This procedure continues until no particles remain from the event, and the clustering algorithm will repeat this procedure for every event in the data structure.

The anti$-k_T$ algorithm ($p = -1.0$) provides the best jet identification technique, due to the near perfect conical structures produced post-clustering. As a consequence of this, anti$-k_T$ is almost exclusively used for the initial identification of jets.

A simple differing choice of p gives jets with different structure and form altogether, such as $\tilde{d}_{ij}$ in Fig.2, and while one algorithm can outperform another there is no comprehensive favourite form of this algorithm for all applications. In this case, we want to recluster jets in order to extract physical information from their substructure when in the presence of a QGP. The τ algorithm, obtained by setting $p = 0.5$, has been shown to be the most suitable for this purpose [8].

2 τ Reclustering and Formation Time

Starting from the uncertainty principle,

$$\Delta E \Delta t \geq \frac{\hbar}{2}, \tag{4}$$

the concept of formation time can be derived via a Lorentz boost to the rest frame of a relativistic particle:

$$t \approx \frac{1}{m}.\frac{E}{m}, \tag{5}$$

where m is the invariant mass of the particle. The decay time of the particle can be given as,

$$\tau_{\text{decay}} = \frac{E}{m^2}. \tag{6}$$

To reach our desired expression, the square of the invariant mass can be expressed as follows:

$$m^2 = (p_{T1} + p_{T2})^2 \approx 2E_1E_2\,(1 - \cos\theta)\,, \tag{7}$$

$$m^2 \approx 2E^2 z\,(1 - z)\,(1 - \cos\theta) \approx E^2 z\theta^2 \tag{8}$$

where the final expression is obtained in the soft-collinear limit. Substituting into (6):

$$\tau_{\text{form}} \approx \frac{1}{Ez\theta^2}, \tag{9}$$

which allows us to relate both the opening angle and the groomed jet mass to τ_{form}. This study compares differences and similarities between the Cambridge-Aachen (C/A, $p = 0$) and formation time ($\tau, p = 0.5$) algorithms when discussing jet reclustering. C/A is an angular-ordered clustering algorithm which reproduces the QCD radiation pattern in vacuum. Meanwhile, the τ algorithm uses the following inverse relation to perform clustering:

$$d_{ij} \approx p_T \theta^2 = \frac{1}{\tau_{form}}, \tag{10}$$

where θ is the angular separation between jets:

$$\theta = \frac{\Delta R}{R}. \tag{11}$$

The τ algorithm has been shown to provide a good correlation between the formation time values extracted from the unclustering sequence and from the primary branch of the parton shower, outperforming the Cambridge-Aachen algorithm [8].

3 Experimental procedure

The Z+jet channel is chosen as the best event topology to examine jet quenching. This is primarily due to the Z boson momentum serving as an estimate to the initial jet momentum. An illustration is shown in Fig.6, which entails a Z+jet event, with the Z boson decaying into a muon-antimuon pair, which is the chosen decay channel for this analysis. As the Z boson and its chosen decay products are colour neutral, the QGP serves as a transparent medium to Z boson interactions, to a good approximation.

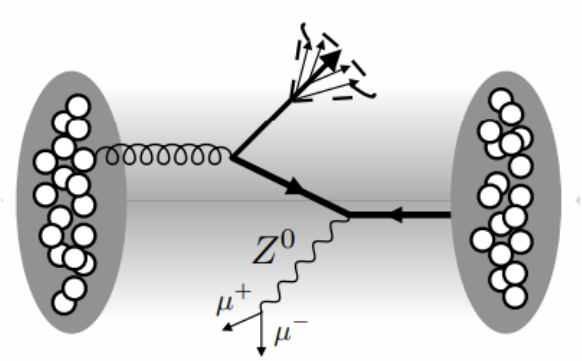

Figure 3. Schematic representing the chosen decay channel: Z+jet, with the Z boson decaying into a muon-antimuon pair. Image courtesy of Pablo Guerrero.

The Z+jet channel events were simulated in both vacuum and medium conditions, using the JEWEL Monte Carlo event generator which includes jet quenching effects [9]. These events were generated without recoils, as to differentiate the energy loss mechanisms from any medium response that a sample containing recoils would involve. From the final event, the two highest p_T muons are selected to reconstruct the Z boson. The leading jet is then selected as the most energetic on the opposing side to the reconstructed Z boson.

3.1 Selection Cuts

The selection cuts provided in Tab.1 follow standard CMS analysis procedures [10]. It is paramount that uninteresting, unimportant events be discarded from the data, as irrelevant data reduces the statistical precision of analyses.

Table 1. Selection cuts applied to discard irrelevant events.

Variable	Cut
$p_{T,Z}$	> 60 GeV
$p_{T,j}$	> 30 GeV
$\lvert\eta\rvert$	< 1.6
$\Delta\phi$	$> \frac{7\pi}{8}$

This is obviously undesirable, so these cuts are made to maximise the certainty in the conclusions drawn for the results discussed in Sec.4.

3.2 Jet Grooming

During certain clustering steps, there might be particularly soft splittings, as a consequence of QCD bremsstrahlung. Such an issue can be resolved via jet grooming [11]. One such method is SoftDrop, which works via comparing each splitting to a predetermined metric z_g:

$$z_g = \frac{\min(p_{T1}, p_{T2})}{p_{T1} + p_{T2}}, \tag{12}$$

where p_{T1} and p_{T2} are the momenta of the leading and sub-leading jets. This method is applied recursively along the primary branch until this condition is satisfied:

$$z_g > z_{\text{cut}} \left(\frac{\Delta R}{R}\right)^{\beta}, \tag{13}$$

where if the energy fraction of the clustering step is not greater than the rightmost expression, this step is discarded from the jet clustering. This removes soft QCD contamination, as well as radiation from underlying events, from the data. Note that we set $z_{\text{cut}} = 0.1$ and $\beta = 0$ in our analysis. A nice bonus of jet grooming is that it also discriminates well against pile-up events (high-likelihood events such as low p_T jet production), so jet grooming is paramount for sensible analysis, as substructure variables are sensitive to pileup [12].

3.3 Data Gathering Procedure

Once SoftDrop has been applied, the groomed jet mass, formation time and opening angles can be steadily calculated from the two-prong structures within the jets [12]. In Sec.4, we will discuss the obtained results, highlighting correlations between variables as well as assessing said variables' suitability for use as selection tools for energy loss purposes.

4 Results

Let us start by analysing the correlations between our variables of interest. For this, we focus on pp events, leaving the PbPb case for the study of energy loss. The data presented in Fig.4 displays the logarithm of the τ_{form} vacuum distribution, ranging from zero to one hundred Fermi. The solid black line represents the results obtained by clustering with the τ clustering algorithm, while the dashed pink

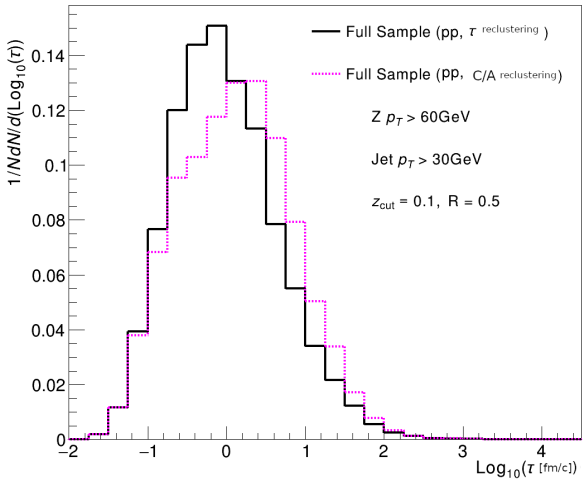

Figure 4. Comparison between clustering algorithms displaying $\text{Log}_{10}(\tau_{\text{form}})$ for both the τ and the C/A clustering algorithms.

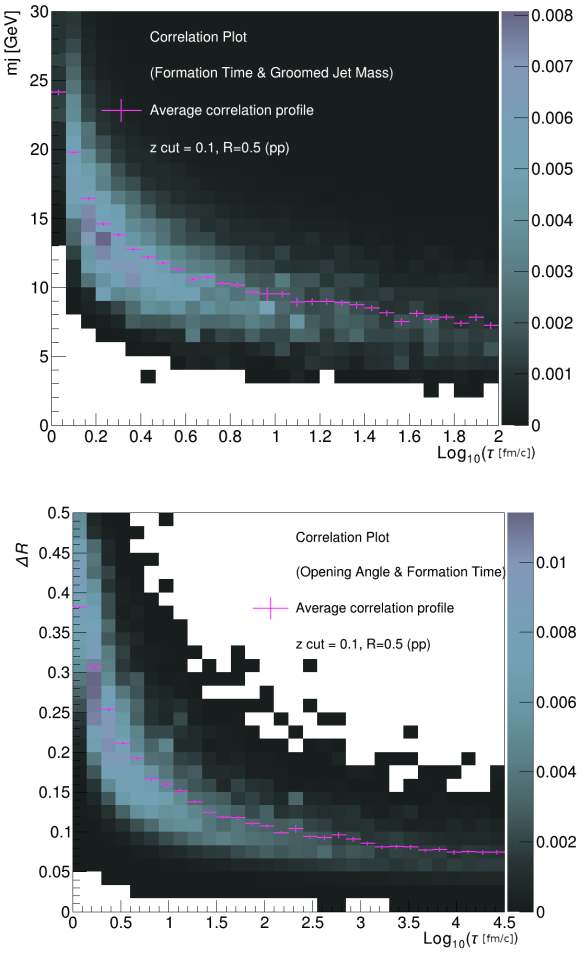

Figure 5. Vacuum correlation plots between groomed jet mass and formation time, as well as opening angle and formation time. Note that white-space also corresponds to a weight of zero.

distribution shows the data clustered via the Cambridge-Aachen algorithm. Fig.4 demonstrates that the τ_{form} distribution does not vary significantly with respect to the τ or the C/A algorithm, although the C/A extracted distribution has a slightly larger mean value: this can be explained via (9), as the z values from C/A clustering are typically smaller than those extracted from the τ algorithm.

Fig.5 displays correlation plots between the substructure variables of interest: the first plot shows the average correlation between the logarithm of formation time and groomed jet mass, while the second plot shows the logarithm of formation time vs opening angle. The pink correlation data points in each plot represent the average correlation between either variable. These correlations support the relations derived in (9), with an inverse relation between τ_{form} and m_j, and an inverse-square relation between τ_{form} and ΔR. While the distributions reproduce these inverse correlations, there are several outliers which disobey this relation: these outliers can be further studied by sampling a quantity sensitive to these variables.

Fig.6 demonstrates the difference in the shapes of the groomed jet mass distributions, τ and C/A compared to their ungroomed counterpart. The solid red line represents the ungroomed mass distribution, while the dashed black line corresponds to jets reclustered via the τ clustering algorithm, and the dashed pink distribution represents data reclustered via the C/A algorithm. The groomed mass distributions will have significantly less events compared to the ungroomed case, but the distributions in Fig.6 are normalised to an inclusive sample to compare structural differences, as opposed to a comparison of sample sizes.

As a result of the removal of soft splittings, the mass peak is reduced for both clustering compared to the ungroomed case. The groomed jet mass distribution have deviations in structure for low masses in the τ and C/A clustering algorithms. Note that this is due to the angular ordering in the C/A algorithm: the first splitting will be a wide emission, which is likely to be softer than a narrow jet, and thus likely removed from the clustering tree. This means that a significant portion of C/A clustered jets will not have their first clustering step meet the imposed z_{cut} condition. Meanwhile, a much larger portion of τ clustered jets will meet the z_{cut} condition, leading to a higher mass peak. The final results of this report do not differ much when using the C/A or τ algorithms: in the jet grooming context, we limit ourselves to show the vacuum τ case, as to highlight the differing mechanisms in a familiar environment.

4.1 Energy Loss Studies

Following on from the vacuum case, we will now consider PbPb collisions, to observe and discuss the effect of QGP on our jet samples. The quantification of energy loss can be performed via the momentum imbalance x_J, the ratio of transverse momenta the jet, $p_{T,j}$, and the Z boson, $p_{T,Z}$, defined as

$$x_J = \frac{p_{T,j}}{p_{T,Z}}. \tag{14}$$

The momentum imbalance gives a method of measuring the modification of the transverse momentum of the jet

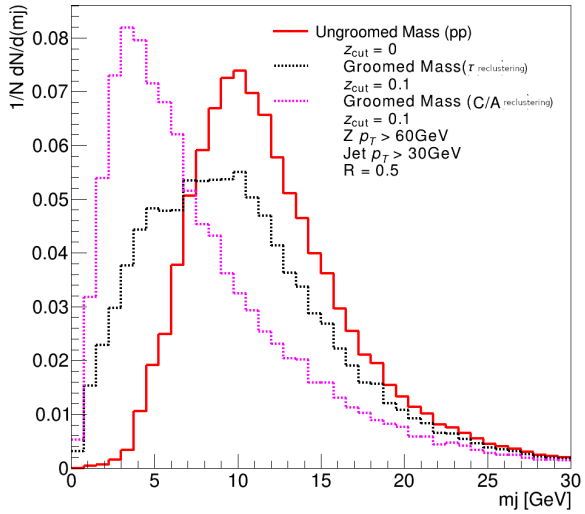

Figure 6. Comparison between groomed mass distributions for the τ and C/A clustering algorithms, as well as the algorithm-independent ungroomed mass distribution. Note that the distributions are normalised to an inclusive sample to compare structure.

between the initial emission of the hard parton and detection. Fig.7 shows the x_J distributions for both vacuum and in-medium models. The solid black line corresponds to the vacuum model, while the dashed-pink line displays in-medium events. The vacuum x_J distribution is, as expected, peaked at unity. This is due to the momentum of the Z boson behaving as a leading-order (LO) estimate for the initial jet momentum. Hence, the minor modifications to the momentum of the jet between production and detection will simply be because of radiation falling out of the jet cone. The comparison between models demonstrates that the in-medium jets have lower momentum values, in their final state, than their vacuum counterparts: this is direct evidence of jet quenching.

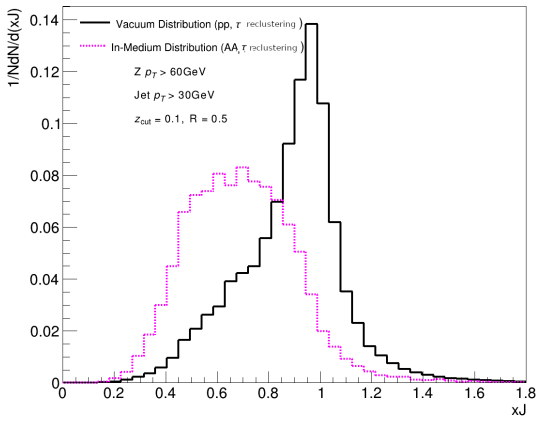

Figure 7. Observation of jet quenching via the modification of a jet's momenta in medium when compared to in vacuum.

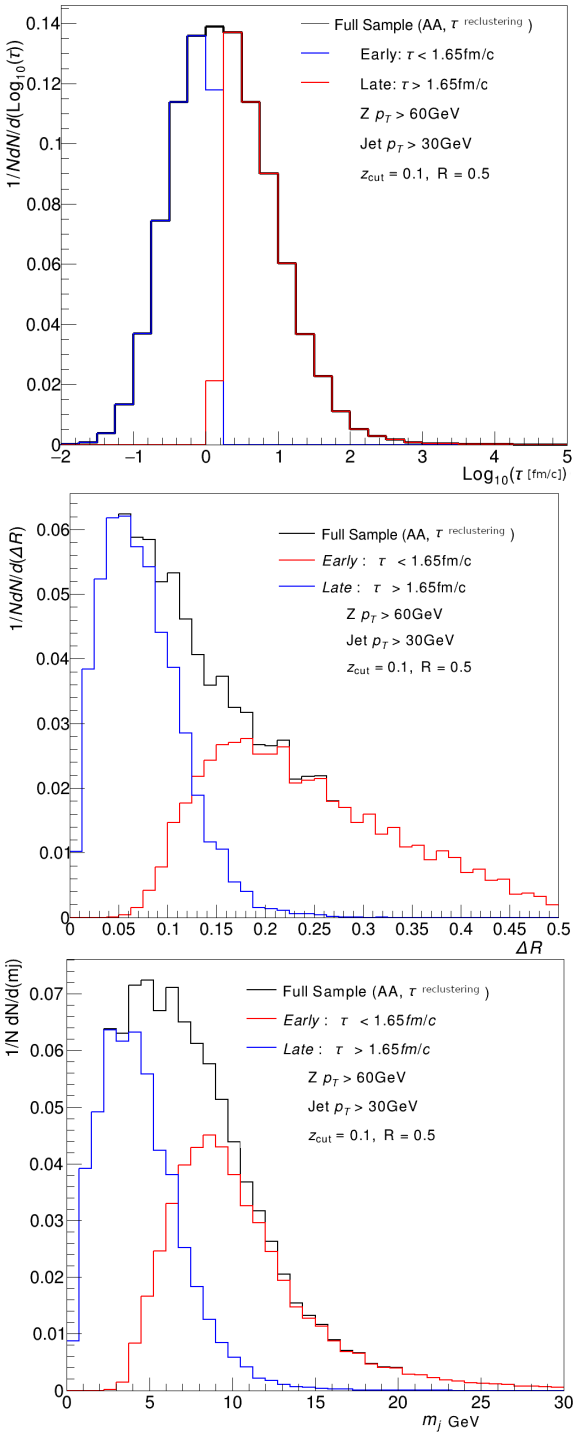

Figure 8. PbPb (in-medium) collision distributions for the formation time, opening angle and groomed jet mass distributions, sampled via a median formation time splitting.

Fig.8 shows the effect of sampling via τ_{form} on both ΔR and m_j distributions. The first plot describes the in-medium logarithmic formation time distribution, while the second and third plots show the ΔR and m_j distributions. We define two populations of jets according to whether their τ_{form} is above or below the median of the distribution. We call these samples late and early jets, respectively. These plots illustrate this procedure in the case of

PbPb collisions, and show the ΔR and m_j distributions corresponding to the selected samples. The blue (red) samples correspond to late (early) jets for both the ΔR and m_j distributions. Sampling early jets corresponds to selecting wider and heavier jets, while the late jets select narrower and lighter jets. Even though the τ_{form} sampling roughly corresponds to median splittings for the other distributions, the splitting is not perfect. The overlap in these distributions consolidate the outliers observed in Fig.5. It is worth noting that the τ_{form} sampling for the opening angle has greater discriminating power than for the groomed jet mass. The difference is due to the overlap of the sampled jets: there is a greater overlap between the early and late jets from the m_j distribution than the ΔR distribution. Hence, the early jets would serve as a better estimate for wide jets than heavy jets, which also means late jets are a better estimate for narrow jets than light jets.

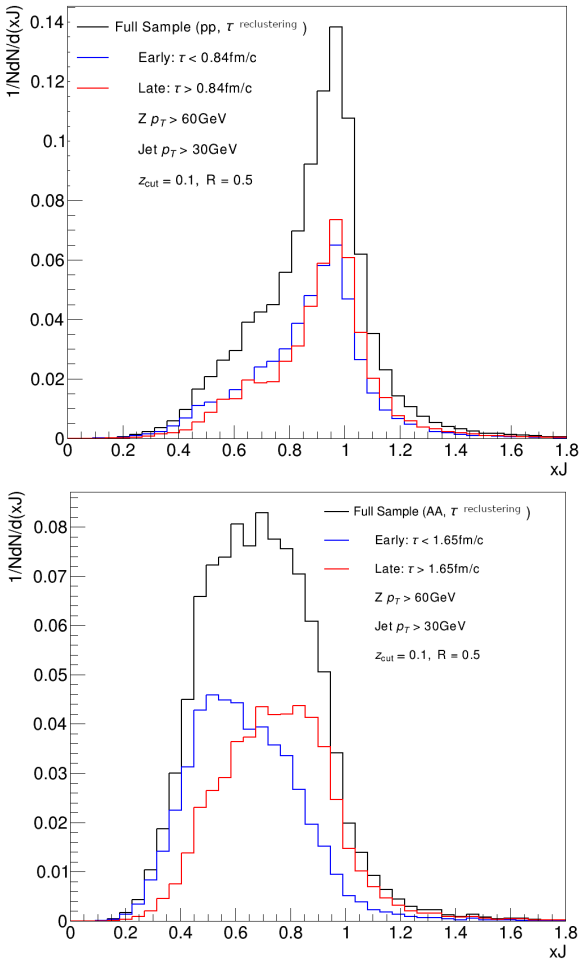

Figure 9. Vacuum and in-medium momentum imbalance spectra sampled via median formation time splitting.

Figs.9,10,11 display the entire x_J range for pp (vacuum; top plot) and PbPb (in-medium; bottom plot) events, sampled via τ_{form}, ΔR and m_j. The purpose of Fig.9 is to investigate the effect of selecting populations of jets that are above or below the median τ_{form}, before observing how this population sampling affects the x_J distribution. Figs.10 and 11 serve as a repetition of this population sampling, but against selections in ΔR and m_j as opposed to τ_{form}. These samplings are performed to determine whether using these variables select equivalent x_J distributions, thus comparing the discriminating power of said variables in the context of energy loss. The groomed jet mass has weak discriminating power when sampling the momentum imbalance spectrum, compared to the formation time and the opening angle selection, which both produce significant variations in the selected groups of jets. In the case of formation time, the sampling can be said to cause early jets to lose more energy due to these jets splitting before the jets produced in the late sample. However, this is a naive assumption, and while it ultimately holds, we need to discuss the fragmentation pattern of the jets to describe the physical motivation behind the shift in the opening angle sampling data. Jets with a harder fragmentation pattern are narrower, hence they lose less energy when interacting with the medium when compared to wider jets, i.e jets with a soft fragmentation pattern [13]. When observing the relation in (9) and Fig.5, we can state that, on average, jets with a harder fragmentation pattern correspond to jets that have larger formation times. From

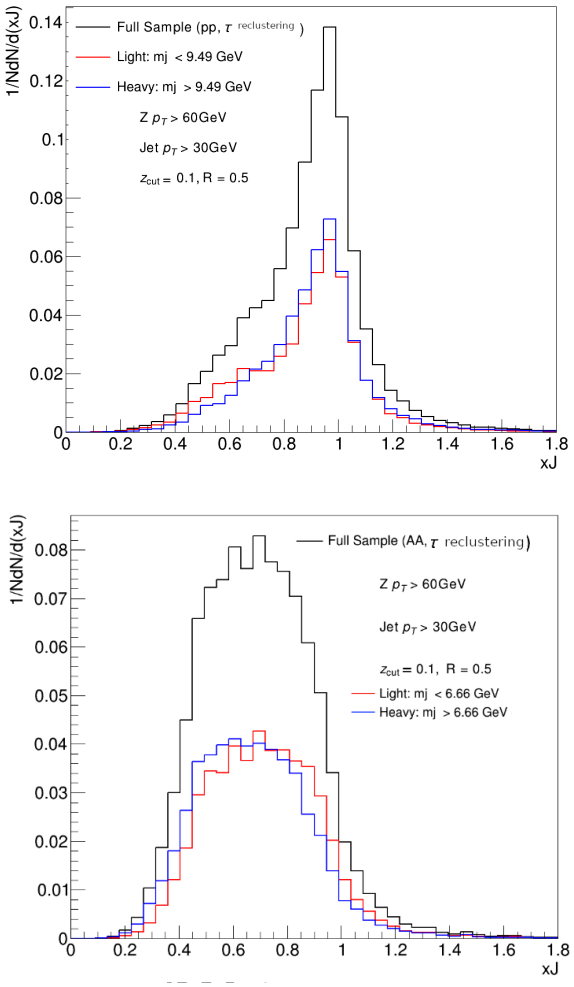

Figure 10. Vacuum and in-medium momentum imbalance spectra split via selection cut in median groomed jet mass.

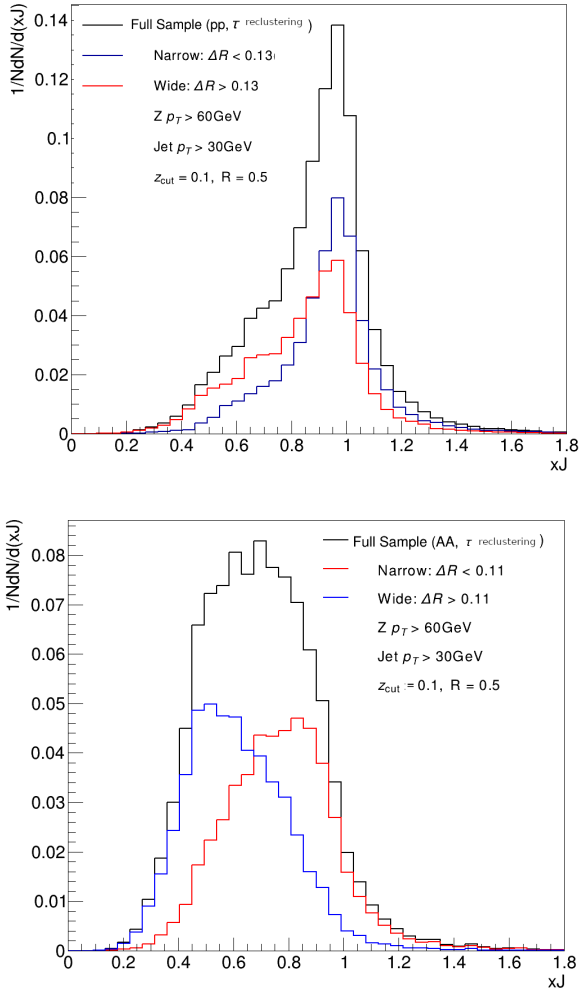

Figure 11. Vacuum and in-medium momentum imbalance spectra split via selection cut in median opening angle.

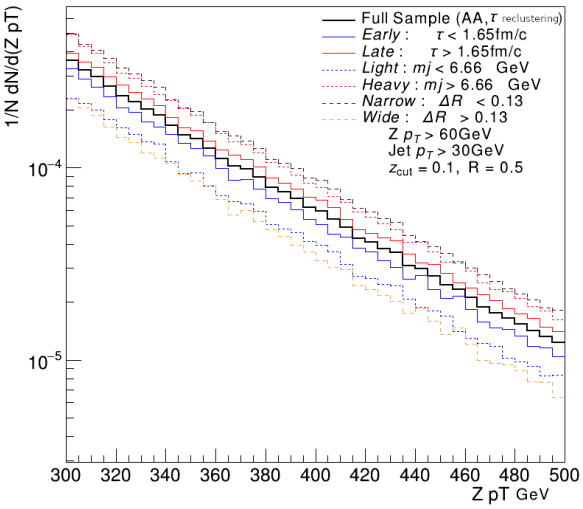

Figure 12. Momentum spectrum of the Z boson. One can assess the selection cuts applied to the data from how they change the overall p_T spectrum.

Figs.9, 10 and 11, we can state that τ_{form} and ΔR outperform m_j as a jet selection tool in energy-loss studies. Note that the modifications observed in the in-medium spectra are not present in the vacuum case! All three vacuum variable samplings do not discriminate between strongly or weakly modified jets, therefore we can conclude that the observed correlations in the in-medium momentum imbalance distributions are a consequence of jet quenching.

Fig.12 displays the momentum distribution of the Z boson produced in our Z+jet events. The solid black line is the inclusive momentum distribution, and the solid red (blue) distribution corresponds to late (early) jets. The dashed red (blue) distribution corresponds to heavy (light) jets, and the dashed brown (yellow) distributions show the narrow (wide) jets. This plot allows us to investigate whether our jet selection (be that according to τ_{form}, ΔR or m_j) induces a bias over the initial momentum of the jet, as we assume it to be equal to $p_{T,Z}$. For example, we can observe that selecting narrower (wider) jets results in a bias towards softer (harder) jets. Observing the Z-boson p_t spectrum above, we conclude that the formation time is significantly less biasing than either the groomed jet mass or the opening angle, consolidating the statement that the formation time is the primary variable that should be discussed when considering future jet quenching studies. While the biasing corresponding to a ΔR or m_j splitting are similar in quantity, this fact does not provide sufficient information to assert any meaningful relation between the variables.

5 Conclusions

The contents of this report delve into the general dependence of energy loss mechanisms on several jet substructure variables, such as τ_{form}, ΔR and m_j. In particular, the investigation on the τ clustering algorithm (p=0.5) in both jet selection and medium-induced effects. The analysis was repeated using the C/A clustering algorithm (p=0), but the results did not differ significantly from the τ clustering case. The suitability of τ_{form} splittings as a proxy for parton shower emissions was discussed extensively in [8]. The JEWEL Monte Carlo event generator was used for the vacuum and medium cases. Events from the Z+jet channel were the sole focus of this work.

The stark difference between the x_J spectra for vacuum and in-medium emissions highlights jet quenching due to interactions with QGP. The primary goal of our energy loss study was to observe whether the population samples selected, for different jet substructure variables, would discriminate against x_J. The procedure consisted of classifying jets according to the values of τ_{form}, ΔR, and m_j corresponding to their first SoftDrop emission. By doing this, we split the total jet population into pairs of samples of equal size, separated by the respective medians of each distribution. Then we examined the contribution of each sample to the overall momentum imbalance distribution, in order to study the sensitivity of each jet class to medium-induced energy loss. Jets with harder fragmentation patters, which correspond to jets with a larger forma-

tion time, lost less energy, on average, when compared to jets with a soft fragmentation pattern. The same conclusion can be made when splitting the x_J distribution with respect to opening angle, with wider jets losing more energy than narrower jets. Splitting x_J via the groomed jet mass does not discriminate between light and heavy jets. Additionally, the ΔR and m_j based sampling induced a significant bias over the entire $p_{T,Z}$ spectrum, which serves as a proxy for the initial jet momentum.

Given the selection bias that both the opening angle and groomed jet mass induce on the momentum of the Z boson, we conclude that the formation time is a more sensible variable to study jet quenching in the context of energy loss studies. Formation time continues to surpass competing variables with significantly less bias from a median splitting, hinting towards the success this variable may hold in future studies.

While the data examined above provides an insight into the behaviour of the physics of jet quenching, other splitting parameters and variables were also considered. The above analysis was repeated for differing z_{cut} values, and events containing jets with a wider radius, $R = 1.0$. The above parameter choices all drew the same conclusions as the data discussed in this work, which strengthens the results discussed in this paper. With regards to future studies, one aspect of the τ algorithm that will be dissected is the relation between the jet clustering history and the parton shower splittings.

Acknowledgements

Thank you LIP for providing me with the opportunity to showcase my skill set, as well as hone in on research interests moving forward. I would like to thank Pablo Guerrero and Liliana Apolinário in particular for their expertise and counsel over the course of this placement.

References

[1] Z. Nagy, D.E. Soper, Physical Review D **98** (2018)

[2] G.P. Salam, Eur. Phys. J. C **67**, 637 (2010), 0906.1833

[3] W. Busza, K. Rajagopal, W. van der Schee, Ann. Rev. Nucl. Part. Sci. **68**, 339 (2018), 1802.04801

[4] R.S. Bhalerao, *Relativistic heavy-ion collisions*, in *1st Asia-Europe-Pacific School of High-Energy Physics* (2014), pp. 219–239, 1404.3294

[5] *https://particlesandfriends.wordpress.com*

[6] L. Cunqueiro, A.M. Sickles, Prog. Part. Nucl. Phys. **124**, 103940 (2022), 2110.14490

[7] L. Apolinário, Y.J. Lee, M. Winn, Prog. Part. Nucl. Phys. **127**, 103990 (2022), 2203.16352

[8] L. Apolinário, A. Cordeiro, K. Zapp, Eur. Phys. J. C **81**, 561 (2021), 2012.02199

[9] K.C. Zapp, Eur. Phys. J. C **74**, 2762 (2014), 1311.0048

[10] S. Chatrchyan et al. (CMS), JINST **3**, S08004 (2008)

[11] A.J. Larkoski, S. Marzani, G. Soyez, J. Thaler, JHEP **05**, 146 (2014), 1402.2657

[12] S. Marzani, G. Soyez, M. Spannowsky, *Looking inside jets: an introduction to jet substructure and boosted-object phenomenology*, Vol. 958 (Springer, 2019), 1901.10342

[13] P. Caucal, E. Iancu, A. Mueller, G. Soyez, PoS **HardProbes2020**, 124 (2021), 2009.01350